JOURNAL OF OPTOELECTRONICS AND ADVANCED MATERIALS Vol. 12, No. 8, August 2010, p. 1684 - 1691

Controllability study of crystallization on whole visible-transparent chalcogenide glasses of GeS_2-Ga_2S_3-CsCl system

C. LIN[a,b], L. CALVEZ[b], B. BUREAU[b], Y. LEDEMI[b], Y. XU[b], H. TAO[a], X. ZHANG[b], X. ZHAO[a]

[a]*Key Laboratory of Silicate Materials Science and Engineering (Wuhan University of Technology), Ministry of Education, Wuhan, Hubei 430070, PR China*

[b]*Laboratoire des Verres et Céramiques, UMR-CNRS 6226, Sciences chimiques de Rennes, Université de Rennes 1, 35042 Rennes Cedex, France*

Phase transformation and nucleation-rate-like curve were firstly determined in chalcogenide glasses based on GeS_2-Ga_2S_3-CsCl system, offering a controlled way to the transparent glass-ceramics with designed-in crystal phases and desired microstructure. The whole visible transparent glass of a composition of $25GeS_2 \cdot 35Ga_2S_3 \cdot 40CsCl$ was specified for a demonstration of the controlled crystallization. The expected crystal phases (Ga_2S_3 crystals) with a very fine size of ~50 nm were achieved successfully, more impressively with a large crystallinity degree of > 80%. An IR-transmitting glass-ceramic with the well improved resistance to the environmental impact was also obtained after a heat-treatment at 350 ^oC for 30h. And the nonlinear evolution of the thermo-mechanical properties for the resultant glass-ceramics is elucidated by the structural investigation employing SEM, XRD, and NMR techniques. The corresponding results would have benefit for the optimization of designing transparent chalcogenide glass-ceramics with highly specialized properties for many potential new applications in IR spectral region.

(Received June 6, 2010; accepted August 12, 2010)

Keywords: Mechanical Properties, Crystallization, Phase Transformations, Chalcogenide glasses, Nucleation rate

1. Introduction

Glass-ceramics of nanocrystalline structure are of growing interest, because of offering promise for many potential new applications as well as providing unique attributes for many current products [1-6]. During the last decades, progress in the development of the oxide based glass-ceramics is remarkable and several products with outstanding mechanical and thermal properties have been used universally [1-4]. However, few investigations deal with chalcogenide glass-ceramics despite their many characteristic advantages [7-9]. In general, glass-ceramics combine the ease of production of glass with much enhanced thermal and mechanical performances, which would be the best choice to solve the intrinsic weakness of the IR-glasses, *e.g.* poor resistance to thermal shock and crack propagation. Furthermore, starting from their wide transmitting spectral region from 0.8 to 12 μm (even up to 20 μm for telluride glasses), chalcogenide glass-ceramics also present interesting characteristics for active optical applications as rare earth (RE) doping [10,11] or permanent second-order nonlinear (SON) optical effects [5, 6] and for passive optical applications [7, 8, 12].

Recently, numerous thermodynamical studies on crystallization of chalcogenide glasses were performed [13-17], but it is still deficient and difficult to conduct a controlled crystallization for desired microstructure with designed-in, highly specialized properties. It is well-known that glass-ceramic technology is based on the controlled nucleation and crystallization of glass. In the last few years, much effect has been devoted to the development of reproducible IR-transmitting glass-ceramics through careful crystallization process, and some good results have been obtained [13, 18, 19]. In spite of this, direct experimental evidence on the crystallization mechanism of chalcogenide glass-ceramics does not exist. It is well-known that knowledge of the nucleation rate as a function of temperature and predication of the resultant crystal phases after crystallization are essential for anticipating phase formation and microstructure in the glass-ceramics technology. Knowing the nucleation rate and phase transformation is important to design a glass-ceramic with a specific property for particular applications, such as for permanent SON optical component and RE-doping solid state laser, where the type and size of resultant crystal phase severely influence the expected performance.

In this study, we describe an effective strategy for achieving controlled crystallization process, and study the improved thermal and mechanical properties in transparent chalcogenide glass-ceramics based on the GeS_2-Ga_2S_3-CsCl system. GeS_2-Ga_2S_3 based glasses were especially selected for their good RE solubility, which is originated from the modified glassy network by the

introduction of Ga [20, 21]. The presence of crystallites would further lower phonon energy environment around RE ions, leading to enhanced quantum efficiency [10, 11]. Consequently, a well understanding of the crystallization behavior in GeS_2-Ga_2S_3 based glasses will have a great contribution to guide candidate materials for solid state lasers. Moreover, the addition of alkali halide increases the bandgap energy E_g by stabilizing the lone pair electrons of sulfur. The incorporation of CsCl, in particular, that Cl bonding to Ge or Ga as non-bridging atoms while the large Cs^+ cations play the role of modifiers situated closer to non-bridging S^-, greatly enlarges the difference of bandgap between the nonbonding and the antibonding levels, making an innovative whole visible-transparent chalcogenide glass [12,22,23]. This newly whole visible-transparent glass presents a great interest for optical application. They could be used both for passive applications (multi-spectral imaging) and active applications for RE doping due to their good transmission in the visible range, increasing optical pumping possibilities. Additionally, based on the previous studies [12,14,24], it can be expected that the gallium would act as a nucleation agent during crystallization to homogeneously precipitate many non-centrosymmetric nanocrystals suitable for SON optical effects. Finally, the most significant in this study, is to open a way to anticipate the crystallized phase based on the glass-forming region and perform a nucleation-rate-like curve for the first time in chalcogenide glass to conduct a controllable crystallization, and then to successfully obtain transparent glass-ceramics with improved thermal and mechanical performances. The principal characteristics specified hereinafter will allow a better comprehension of the crystallization in chalcogenide glasses.

2. Experimental

Bulk glasses in GeS_2-Ga_2S_3-CsCl system were synthesized using the polycrystalline germanium (5N), Gallium (5N), sulfur (5N) and CsCl (3N) as starting materials. Appropriate quantity (10 g) of each component was weighed according to the stoichiometric glass composition and introduced into a silica tube, which was pumped to a vacuum of about 10^{-3} Pa, and then sealed. The sealed silica tubes were put into a rocking furnace and heated to 850-920 ^oC at a rate of 2 ^oC/min. The mixture was melted at this temperature for about 10 h and quenched in cold water. Subsequently, the obtained glass rod was annealed below glass transition temperature (T_g) for 3h to minimize inner stress, and finally slowly cooled down to room temperature. The glass disks (Φ10 mm×1.2 mm) were cut from the glass rods and polished to optical quality on both sides.

The characteristic temperatures of as-prepared glass were determined by differential scanning calorimeter (DSC, Type: DSC Q20 Thermal Analysis). Hermetic aluminum pans with ~10 mg samples were heated from room temperature until crystallization completed under a N_2 atmosphere in the DSC machine. The glass transition temperature T_g, crystallization peak temperature T_p, integral area of crystallization peak (CP), and peak height ($(\delta T)_p$) were obtained using the microprocessor of thermal analyzer. In addtion, DSC also has been shown to be a rapid and convenient means for determining nucleation-rate-like curves of glasses, especially the temperature range where nucleation occurs and the temperature where the nucleation rate is a maximum [25-27]. Unlike the time-consuming, traditional method, in this case, a small amount of glass sample first was nucleated at different temperatures for a fixed time before being crystallized (via heating at a fixed rate) in the DSC machine. It is well known that the number of nuclei developed in a particular volume of a glass at different temperatures would have a temperature dependence identical with that of the nucleation-rate curve, provided that the nucleating time at each temperature is constant. The applicability of DSC peak height ($(\delta T)_p$) instead of nucleation rate has been justified from both experimental results and theoretical considerations [25-29]. Thus a plot of $(\delta T)_p$ as a function of the nucleation temperature (T_n), produced a nucleation-rate-like curve that, to a reasonable degree of accuracy, determines the temperature range for nucleation and the temperature of the maximum nucleation rate.

Based on the DSC results, the crystallization process was conducted in a ventilated furnace by heating at a rate of 2 ^oC/min to a specific temperature, T_{HT}, preserving for various durations, and then cooling slowly to room temperature. The transmission spectra of as-prepared and heat-treated samples were recorded with a CARY5 double-beam spectrophotometer (Varian, Mulgrave, Vic., Australia) in visible and near-IR (Vis-NIR) spectral region, and a Bruker Vector 22 spectrophotometer (Bruker Optics, Wissenbourg, France) in the mid-IR region ranging from 2 μm to 12.5 μm, respectively. The size or morphology of crystals was observed by scanning electronic microscopy (SEM) with the technique described elsewhere [15], in a fresh crack created on the glass surface. The crystalline phases present in the heat-treated samples were identified using a Philips PW 3020 diffractometer (Voltage: 40 kV; current: 20 mA; Cu $K\alpha$) with a step width of 0.02 ^{o}, and confirmed reciprocally by the ^{133}Cs and ^{71}Ga NMR experiments. The ^{133}Cs spectra were recorded at room temperature on an Avance 300 Bruker spectrometer operating at 39 MHz with a 4 mm magic angle spinning (MAS) probe spinning at 10 kHz. And the ^{71}Ga (spin I =3/2) spectra were recorded at 91.5 MHz with a static probe. The decomposition of the experimental spectra was performed using the Dmfit#20080317 Version of the Dmfit software [30,31].

To learn if the thermo-mechanical properties improved after crystallization, thermal expansion coefficient (TEC) α, Vickers hardness, and fracture toughness, etc., were measured in the as-prepared and crystallized glasses. TEC was determined using a TMA

2940 Calorimeter (TA Instruments) at a heating rate of 2 °C/min from room temperature to 200 °C with an error of 2×10^{-7} K^{-1}. Vickers microindenter (Matsuzawa VMT-7S, Matsuzawa Co. Ltd., Tokyo, Japan) was used to obtain the hardness with a charge of 100g for 5s. All the characteristics were averaged over measurements on 10 indentations per sample with an error of 2 kg·mm^{-2}. Fracture toughness (K_c) was then calculated by the modified Palamqvist's method [32] using the following equation:

$$K_c = 0.016\left(\frac{E}{H}\right)^{1/2}\frac{P}{c^{3/2}} \quad (1)$$

where H is Vickers hardness, P (in newtons) is the load applied on the indenter, c (m) is half the mean length of the two radical cracks (tip to tip), and E (GPa) is Young's modulus, obtained by measuring the ultrasound propagation speed in the glass. Density, ρ, was measured using the Archimedes technique which consists in comparing the difference of the sample weight in the air and in a solvent. A Metler Toledo XS64 balance was used with distilled water as solvent.

3. Results and discussion

3.1 Determination of Phase Transformation and Nucleation Rate

A fairly large glass-forming region of GeS_2-Ga_2S_3-CsCl system is shown in Fig. 1, which was firstly reported by Tver'yanovich, et al. [33]. According to the DSC analysis, we can classify this glass-forming region into two categories [34]: very stable glasses (no exothermal peak or ΔT=T_c-T_g >170 °C) and sub-stable glasses as shown in Fig. 1. Four different compositions of A $80GeS_2{\cdot}20Ga_2S_3$ [14], B $25GeS_2{\cdot}35Ga_2S_3{\cdot}40CsCl$, C $50GeS_2{\cdot}12.5Ga_2S_3{\cdot}37.5CsCl$, and D $65GeS_2{\cdot}25Ga_2S_3{\cdot}10CsCl$ [35], were selected for this crystallization study, respecting such criteria as sub-stable glasses to ensure an easy separation of crystal phases. Subsequent to an adequate crystallization process, XRD measurement has been performed to show that different crystal phases were separated out from the glassy matrix as indicated in Fig. 2. It is seen that Ga_2S_3 particles were crystallized in the glasses of compositions A and B. Similarly in our previous work [35], the base glass of composition D also crystallized particles of Ga_2S_3 during the initial heat-treatments. Besides, it can be observed that another kind crystal of CsCl was also precipitated in the base glass of composition C. Therefore, it can be concluded that the phase transformation of the sub-stable glasses is to separate out the glassy phase incompatible with the host glass, leading the composition of residual glassy matrix to the very stable glass region. It behaves as the green arrow portrayed in Fig. 1. This belief would be of great reference value for designing glass-ceramics with designed-in, highly specialized crystals by controlling the composition of base glasses.

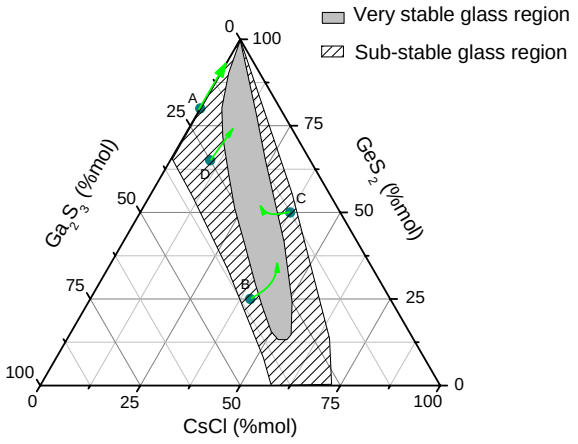

Fig. 1. Glass-forming domain of the GeS_2-Ga_2S_3-CsCl system with the compositions for crystallization investigations: A $80GeS_2{\cdot}20Ga_2S_3$ [14], B $25GeS_2{\cdot}35Ga_2S_3{\cdot}40CsCl$, C $50GeS_2{\cdot}12.5Ga_2S_3{\cdot}37.5CsCl$, and D $65GeS_2{\cdot}25Ga_2S_3{\cdot}10CsCl$ [35], respectively. The green arrows show the compositional tendency of the residual glass matrix during crystallization process.

In addition to the phase transformation described by Fig. 1, knowledge of nucleation rate is also essential for the preparation of glass-ceramics with desired microstructure through controlled nucleation and crystallization. Before the attempt for getting the pseudo-nucleation rate curve, two requirements should be considered [28]: first, all nucleation is completed prior to crystal growth; second, only does one transformation mechanism occur during crystallization. According to the DSC results (not shown here), the presence of two or more crystallization peaks indicates distinct phase transformations or different crystallization mechanism in the base glasses of compositions of A, C and D. Hereby, only could base glass of composition B ($25GeS_2{\cdot}35Ga_2S_3{\cdot}40CsCl$) be specified for measurements of the nucleation-rate-like curve. In addition, this glass also was selected due to its whole visible-transparent spectral region and proper chemical stability. Subsequently, nucleation-rate-like curves of glass B described by $(\delta T)_p$ vs. T_n are shown in Fig. 3, which are normalized by $[S(T_n)-S(0)]/[S(max)-S(0)]$, where S represents $(\delta T)_p$, $S(0)$ is delegated for that of an as-prepared glass, $S(T_n)$ for that of the glass nucleated at any temperature, and $S(max)$ for the maximum value among all the glasses measured, respectively. At the first sight, the profile for three different durations is almost the same, indicating the shape

of nucleation-rate-like curve simply has a temperature dependence, and meanwhile validating themselves reciprocally. Fig. 3 further shows that the temperature where the nucleation can occur in the glass B ranges from 310 °C to 370 °C and the nucleation rate reaches a maximum at 340 ± 5 °C. In the curve of glass sample heat-treated at different temperatures for 4h, the temperature range of nucleation (T_n^{range}) is slightly narrowed at the high-temperature side, compared with the other two curves. This small difference of T_n^{range} (~10 °C) is attributed to the considerable overlap of the nucleation and crystal growth curves for this glass sample. Because the peak height is proportional to both the maximum phase transformation rate and the volume fraction crystallized during the DSC run, any small amount of crystallization occurring during the nucleating heat-treatment will decrease the peak height, $(\delta T)_p$ [29]. Fig. 4(a) displays the curves of the integral area of CP vs. the nucleating temperature for three different times (1.5h, 2.5h, and 4h). One can derive from Fig. 4 a) that no observable crystal growth is involved during the short time nucleating heat-treatments of 1.5h and 2.5h, whereas the crystal growth which results in a decreasing volume of residual glass matrix shifts the high-temperature side of T_n^{range} to low temperature for the 4h nucleated samples. Consequently, Fig. 4 b) schematically describes the overlap between nucleation and growth rate curves, and reveals the reason for selecting a single-stage heat-treatment at temperature T_H (350 °C) for the subsequent crystallization process.

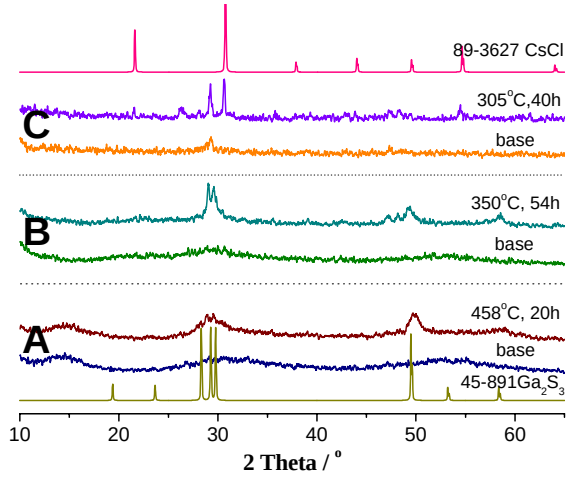

Fig. 2 XRD patterns of glasses and glass-ceramics with three different compositions: A $80GeS_2{\cdot}20Ga_2S_3$ [14], B $25GeS_2{\cdot}35Ga_2S_3{\cdot}40CsCl$, and C $50GeS_2{\cdot}12.5Ga_2S_3{\cdot}37.5CsCl$ base glasses and glasses crystallized at different temperatures for appropriate times, respectively.

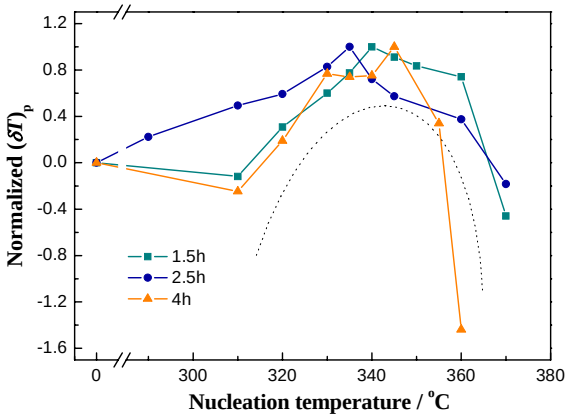

Fig. 3 Nucleation-rate-like curve of glass B ($25GeS_2{\cdot}35Ga_2S_3{\cdot}40CsCl$) described by normalized $(\delta T)_p$ vs. T_n for different times: 1.5h, 2.5h, and 4h, respectively. Dash line is a guide to eye. (For a DSC run, sample weight is 10 mg, particle size is >500um, and DSC heating rate Φ is 20 °C/min.).

3.2 Characterization of the Resultant Glass-Ceramics

Based on the suggestions from the above analysis, a validation was performed in the base glass of composition B ($25GeS_2{\cdot}35Ga_2S_3{\cdot}40CsCl$), and the subsequent ceramization was carried out at a specific temperatures T_H=350 °C for various durations. A set of crystallized samples with a thickness of 1.2 mm were obtained, as presented in Fig. 5. The spectra of Vis-NIR transmission, which are very sensitive to the presence of crystals, are shown in Fig. 6 a). As indicated in Table 1, it is clear that the cut-off edge of short wavelength is red shifted as a function of annealing time. In spite of the visible opacity of the samples crystallized for more than 30h as shown in Fig. 5, fortunately, they are still transparent ranging from 2 μm to 11 μm (Fig. 6 b)), indicating the suitable and potential applications in mid-IR spectral region. More impressively, the degree of crystallinity exceeds ~80% in the glass crystallized for 30h, which remains its maximal IR transmittance. This phenomenon can be well elucidated by Hendy's equation [36] which shows the importance of having particles of refractive index different from that of the matrix glass smaller than 50 nm (as indicated by the SEM images of Fig. 7) to minimize scattering loss. Also indicated in Fig. 7, the size and amount of nano-particles increased simultaneously with the elongation of heat-treatment. Noticeably, the crystal grows slowly from 10 nm to 50 nm, meanwhile the nucleation also takes places so as to achieve approximately 80% crystallinity degree. It is the exact evidence to confirm that the heat-treated temperature of 350 °C is located at the overlap of nucleation and crystal growth rate curves as shown in Fig. 4 b).

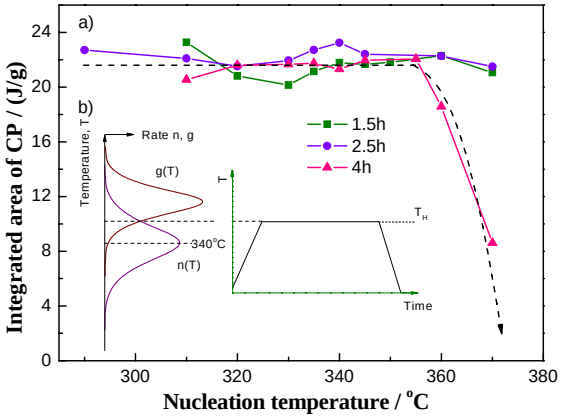

Fig. 4 a) Integral area of DSC peak vs. the nucleating temperature for glass B nucleated at different temperatures for three different times: 1.5h, 2.5, and 4h, respectively. The inset b) is a sketch of single-stage heat treatment for the glass B, showing the overlap of nucleation and crystal growth curves. The dash lines are guides to eye.

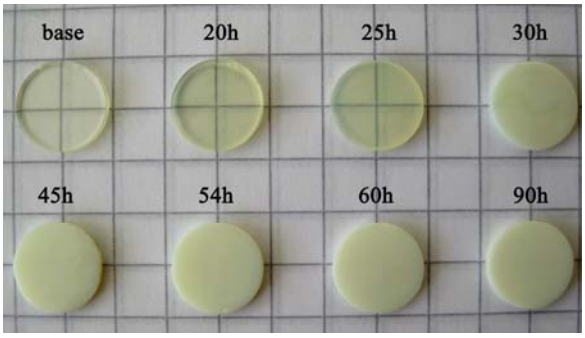

Fig. 5 A set of glasses B crystallized at 350 °C for different durations: 0 (base) to 90h.

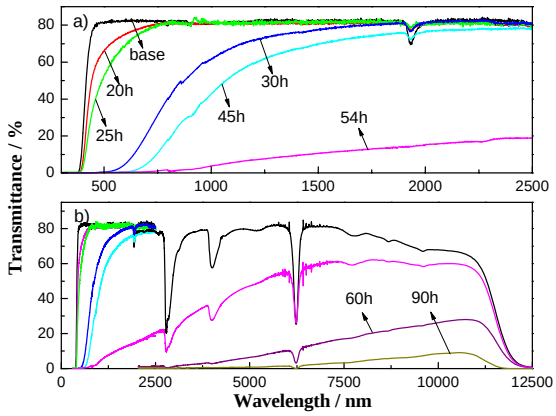

Fig. 6. Transmission spectra of the glasses B heat treated at 350 °C for 0 h to 90 h in different spectral regions: a) Vis-NIR and b) whole transmitting spectral regions.

Table 1 Some physical and thermo-mechanical properties of the glass and glass-ceramics of composition B.

Samples	Cut-off edge (half of tans.) (±1 nm)	Density, ρ (±0.002 g/cm^3)	Hardness, H_v (±2 Kg ·mm^{-2})	Fracture toughness, K_c (±0.005 MPa·m$^{-1/2}$)	TEC, α (±1×10^{-7} K^{-1})
Base	410	3.165	130.00	0.405	205
20h	430	3.162	127.58	0.393	205
25h	461	3.174	132.96	0.457	203
30h	798	3.235	152.01	No crack	173
45h	956	3.295	150.59	No crack	180
54h	3440	3.315	152.24	No crack	228
60h	7005	3.324	142.34	No crack	197
90h	8070	3.366	120.70	No crack	258

To investigate whether the resistance to the environmental impact improved after the crystallization process, some thermo-mechanical properties of the obtained samples were studied in detail, and the results are listed in Table 1. The precipitated crystals greatly inhibit the crack propagation leading to increasing fracture toughness even to no observable cracks with long heat-treatments. However, the evolution of other thermal and mechanical properties is more complicated, especially for the crystallized glass with a long heat-treatment (>30 h). Combined with the results of XRD [35] and NMR (Fig. 8 and 9), it can be ascribed to structural change of residual glass matrix originated from the precipitation of different crystals during the long crystallization process. ^{71}Ga NMR spectra of the obtained glass-ceramics recorded in static mode are presented with the variation of heat-treated times in Fig. 8. Since the initial crystallization process, a small bump attributed to the Ga-related crystalline state grows gradually from the broad base profile which is originated from the amorphous phase. XRD pattern in Fig. 2 indicates the small bump is ascribed to the Ga_2S_3 crystallites. In addition, it is observable that the progressive bump locates at the same position as the glass D crystallized for 65h, in which the Ga atoms were well-crystallized in the matrix [35]. The small bump of profile, not a sharp peak, is possibly due to the very fine size (50 nm) of Ga_2S_3 particles. Furthermore, the behavior of cesium during the crystallization process is revealed by the ^{133}Cs NMR spectra as shown in Fig. 9. It is seen that no observable change happens for the crystallized glass of composition B at the initial 30h heat-treatment. All of them exhibit typical broad bands of the glassy state. Subsequent to the 90h and 120h heat-treatment, the Cs-related band shifts to low chemical shift (from -81 ppm to -97 ppm), keeping away from that of crystalline CsCl. It

is notable that the shift behavior between B base glass and glass-ceramics is similar to that of D base glass and glass crystallized for 65h, in which a crystalline phase containing cesium has been confirmed [35]. Therefore, after quite long heat-treatment of glasses B, the cesium is incorporated into a complex crystalline phase in which Cs^+ are surrounded by S^{2-} and Cl^- anions.

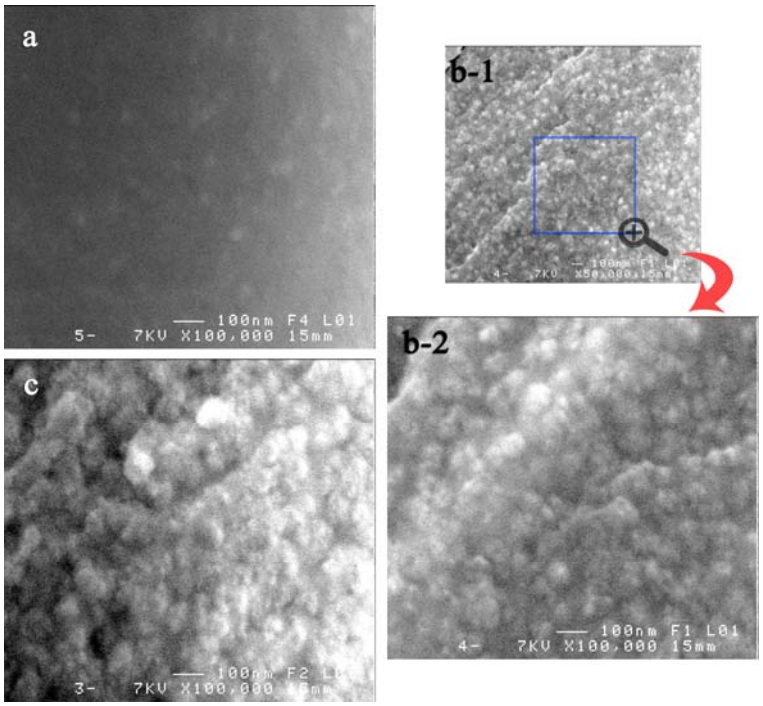

Fig. 7 SEM images for glasses B crystallized at 350 °C for different durations: a) 25h ×100,000, b-1) 30h ×50,000, b-2) 30h ×100,000, and c) 54h ×100,000, respectively.

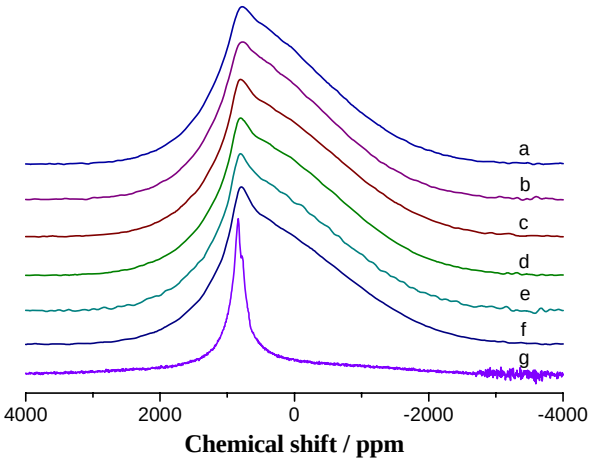

Fig. 8 ^{71}Ga NMR spectra of glasses B crystallized at 350 °C for different durations (a 0h, b 20h, c 30h, d 45h, e 90h, f 120h), and glass D crystallized at 425 °C for 65h (g) [35], respectively.

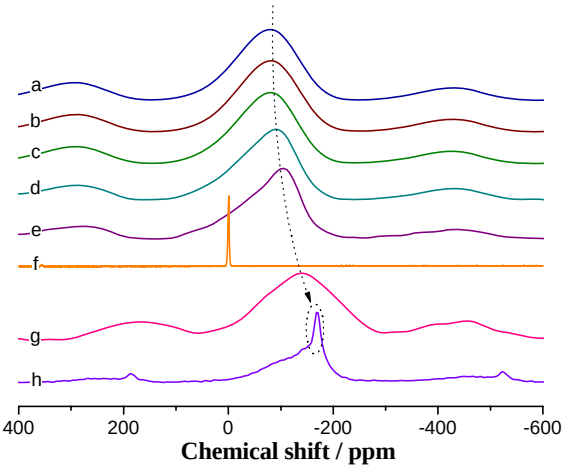

Fig. 9 ^{133}Cs NMR spectra of glasses B crystallized at 350 °C for different durations (a 0h, b 20h, c 30h, d 90h, e 120h), commercial CsCl (f), and D glass crystallized at 425 °C for 0h (g) and 65h (h) [35], respectively.

In favor with the structural investigation, the odd variation of thermal and mechanical properties in B glass-ceramics can be elucidated as follows. The increase of density indicates that the nonlinear evolution of TEC should be originated from the structural changes in the residual glassy matrix, so does for the behavior of hardness. One can see that the presence of Ga_2S_3 crystallites or the divergency of edge-shared $[GaS_xCl_{4-x}]$ structural units from the glassy matrix results in increasing H_v and decreasing TEC. And then, for long annealing times of 60h and 90h, $[GeS_4]$ tetrahedral units who play a predominant role as glassy former were also precipitated (demonstrated by XRD patterns in ref. [35]). Additionally, the network modifier of cesium is also separated out from the residual glass by the formation of Cs-related crystals. Similar to a ceramic, its residual glassy framework is almost wrecked by formation of a large amount of crystals, wherefore resulting in these deteriorated performances. Thus, the glassy network of B glass-ceramics is almost collapsed, leading to the unusual behavior of hardness and TEC.

4. Conclusions

Based on the glass-forming region, phase transformation was determined by the investigation of crystallization on four different base glasses in GeS_2-Ga_2S_3-CsCl system. It is indicated that the phase transformation of the sub-stable glasses is to separate out the glassy phase incompatible with the host glass, leading the composition of residual glassy matrix to the very stable glass region. Nucleation-rate-like curve was also firstly determined in chalcogenide glasses based on GeS_2-Ga_2S_3-CsCl system by the DSC technique. The temperature for maximum nucleation is determined at 340 ± 5 ^oC for the glass with composition B ($25GeS_2{\cdot}35Ga_2S_3{\cdot}40CsCl$). Temperature where the nucleation can occur in the glass B ranges from 310 ^oC to 370 ^oC. And then, a heat-treated temperature T_H of 350 ^oC located at the overlap between nucleation and crystal growth rate curves was specified for the subsequent crystallization process of B glasses.

Based on the information of phase transformation and nucleation-rate-like curve, a controllable crystallization was performed in the base glass of composition B ($25GeS_2{\cdot}35Ga_2S_3{\cdot}40CsCl$). A set of reproducible glass-ceramics with high transparency in the mid-IR region were obtained by the heat-treatments at 350 ^oC for different durations. An IR-transmitting glass-ceramic with the best resistance to the environmental impact has been achieved after 30h heat-treatment, which has 15.6% decrease for TEC, 16.9% increase for hardness, and the maximum resistance to the crack propagation. According to the structural investigation by SEM, XRD, and NMR techniques, the nonlinear change of the thermo-mechanical properties for the resultant glass-ceramics was elucidated by the structural evolution in glassy matrix.

Consequently, through choosing a proper composition of base glass based on the insight of phase transformation, expected crystallites would be specified in the obtained glass-ceramics for offering a specific application. Furthermore, to minimize scattering for keeping a wide range of transparency, crystallites of small size can be well controlled by the knowledge of nucleation-rate-like curve. It is of great guiding significance for a controlled fabrication of IR glass-ceramics for passive and active applications.

Acknowledgements

This work was partially funded by Natural Science Foundation of China (NSFC) (60808024), the National Science Foundation (NSF) of Hubei Province, and the Program for Changjiang Scholars and Innovative Research Team (PCSIRT, No. IRT0547), Ministry of Education, China.

Reference

[1] H. Hijiya, T. Kishi, A. Yasumori. J Ceram Soc JPN;**117**, 120 (2009).
[2] F. Torres, Y. Benino, T. Komatsu, C. Lavelle. J Mater Sci **36,** 4961 (2001).
[3] Y. Takahashi, Y. Benino, T. Fujiwara, T. Komatsu. Appl Phys Lett **81**, 223 (2002).
[4] G. H. Beall, L. R. Pinckney. J Am Ceram Soc **82**, 5 (1999).
[5] C. Lin, H. Tao, R. Pan, X. Zheng, G. Dong, H. Zang, X. Zhao. Chem Phys Lett **460**, 125 (2008).
[6] C. Lin, H. Tao, X. Zheng, R. Pan, H. Zang, X. Zhao. Opt Lett **34,** 437 (2009).
[7] L. Calvez, H. Ma, J. Lucas, X. Zhang. J Non-Cryst Solids **354**, 1123. (2008) .
[8] X. Zhang, L. Calvez, V. Seznec, H. Ma, S. Danto, P. Houizot, C. Boussard-Plédel, J. Lucas. J Non-Cryst Solids, **352**, 2411 (2006).
[9] X. Zhang, H. Ma, J. Lucas. J Non-Cryst Solids **337,** 130 (2004).
[10] V. Seznec, H. Ma, X. Zhang, V. Nazabal, J.L. Adam, X. Qiao, X. Fan. Opt Mater;**29**, 371 (2006).
[11] R. Balda, S. García-Revilla, J. Fernández, V. Seznec, V. Nazabal, X. Zhang, J. L. Adam, M. Allix, G. Matzen. Opt Mater **31**, 760 (2009).
[12] L. Calvez, H. Ma, J. Lucas, X. Zhang. Adv Mater **19**, 129 (2007).
[13] S. Zhu, H. Ma, M. Matecki, X. Zhang, J.L. Adam, J. Lucas. J Non-Cryst Solids **351**, 3309 (2005).
[14] C. Lin, L. Calvez, M. Rozé, H. Tao, X. Zhang, X. Zhao. Appl Phys A-Mater 2009;DOI:10.1007/s00339-009-5304-1.
[15] L. Calvez, H. Ma, J. Lucas, P. Glouannec, X. Zhang. J Non-Cryst Solids **353,** 4702 (2007).

[16] X. Liu, S. Shen, A. Jha. J Mater Res **20**, 856 (2005).
[17] J. J. Mecholsky Jun, C.T. Moynihan, P.B. Macedo, G.R. Srinivasan. J Mater Sci **11**, 1952 (1976).
[18] L. Calvez, M. Rozé, Y. Ledemi, H. Ma, J. Lucas, M. Allix, G. Matzen, X. Zhang. J Ceram Soc JPN; **116,** 1079 (2009).
[19] H. Ma, L. Calvez, B. Bureau, M. Le Floch, X. Zhang, J. Lucas. J Phys Chem Solids; **68**, 968 (2007).
[20] Z.G. Ivanova, E. Cernoskova, Z. Cernosek. J Phys Chem Solids **68**, 1260 (2007).
[21] Z.G. Ivanova, Z. Aneva, Z. Cernosek, E. Cernoskova, V.S. Vassilev. J Mater Sci.-Mater EL **14,** 761 (2003).
[22] L. Calvez, P. Lucas, M. Rozé, H. Ma, J. Lucas, X. Zhang. Appl Phys A-Mater;**89,** 183 (2007).
[23] Y. Ledemi, L. Calvez, M. Rozé, X. Zhang, B. Bureau, M. Poulain, Y. Messaddeq. J Optoelectron Adv Mater. **9,** 3751 (2007).
[24] M. Rozé, L. Calvez, Y. Ledemi, M. Allix, G. Matzen, X. Zhang. J Am Ceram Soc **91,** 3566 (2008).
[25] C.S. Ray, D.E. Day. J Am Ceram Soc **80**, 3100 (1997).
[26] C.S. Ray, X. Fang, D.E. Day. J Am Ceram Soc **83,** 865 (2000).
[27] C.S. Ray, D.E. Day. J Am Ceram Soc **73**, 439 (1990).
[28] M.C. Weinberg. J Am Ceram Soc;**74,** 1905 (1991).
[29] X.J. Xu, C.S. Ray, D.E. Day. J Am Ceram Soc **74** 909 (1991).
[30] B. Bureau, J. Troles, M.L. Floch, P. Guénot, F. Smektala, J. Lucas. J Non-Cryst Solids **319,** 145 (2003).
[31] D. Massiot, F. Fayon, M. Capron, I. King, S.L. Calvé, B. Alonso, J.O. Durand, B. Bujoli, Z. Gan, G. Hoatson. Magn Reson Chem **40**, 70 (2002).
[32] J.P. Guin, T. Rouxel, J.C. Sanglebœuf, I. Melscoët, J. Lucas. J Am Ceram Soc **85**, 1545 (2002).
[33] Y. S. Tver'yanovich, V.V. Aleksandrov, I. V. Murin, E.G. Nedoshovenko. J Non-Cryst Solids **256&257,** 237 (1999).
[34] F. Xia, X. Zhang, J. Ren, G. Chen, H. Ma, J.L. Adam. J Am Ceram Soc **89**, 2154 (2006).
[35] Y. Ledemi, B. Bureau, L. Calvez, M.L. Floch, M. Rozé, C. Lin, X. Zhang, M. Allix, G. Matzen, Y. Messaddeq. J Chem Phys B**113**, 14574 (2009).
[36] S. Hendy. Appl Phys Lett **81,** 1171 (2002).

*Corresponding author: linchanggui@gmail.com